Effect of asymmetry on the loss of chaos synchronization

Sang-Yoon Kim* and Woochang Lim
Department of Physics, Kangwon National University, Chunchon, Kangwon-Do 200-701, Korea
(Received 26 October 2000; published 15 June 2001)

We investigate the effect of asymmetry of coupling on the bifurcation mechanism for the loss of synchronous chaos in coupled systems. It is found that only when the symmetry-breaking pitchfork bifurcations take part in the process of the synchronization loss for the case of symmetric coupling, the asymmetry changes the bifurcation scenarios of the desynchronization. For the case of weak coupling, pitchfork bifurcations of asynchronous periodic saddles are replaced by saddle-node bifurcations, while for the case of strong coupling, pitchfork bifurcations of synchronous periodic saddles transform to transcritical bifurcations. The effects of the saddle-node and transcritical bifurcations for the weak asymmetry are similar to those of the pitchfork bifurcations for the symmetric-coupling case. However, with increasing the ''degree'' of the asymmetry, their effects change qualitatively, and eventually become similar to those for the extreme case of unidirectional asymmetric coupling.

DOI: 10.1103/PhysRevE.64.016211 PACS number(s): 05.45.Xt

I. INTRODUCTION

In recent years, the phenomenon of chaos synchronization has become a field of intensive research. When coupled chaotic systems attain a state of synchronization, a synchronous chaotic motion occurs on an invariant subspace of the whole phase space [1–3]. In particular, this chaotic synchronization has attracted much attention, because of its potential practical application in secure communication [4].

An important question in this field concerns stability of chaos synchronization with respect to a perturbation transverse to the invariant subspace [5]. If it is transversely stable (i.e., its transverse Lyapunov exponent is negative), then the synchronous chaotic state on the invariant subspace becomes an attractor in the whole phase space. Such transverse stability of the synchronous chaotic attractor (SCA) is intimately associated with transverse bifurcations of periodic saddles embedded in the SCA [6–10]. If all periodic saddles embedded in the SCA are transversely stable, the SCA becomes asymptotically stable (i.e., Lyapunov stable and attracting in the usual topological sense). For this case, we have ''strong'' synchronization. However, as the coupling parameter passes through a threshold value, a periodic saddle embedded in the SCA first becomes transversely unstable through a local bifurcation. After this first transverse bifurcation, a dense set of locally repelling ''tongues'' opens from the transversely unstable repeller and its preimages, and hence, trajectories falling in these tongues are repelled from the invariant subspace. Thus, loss of strong synchronization begins with the first transverse bifurcation, and then we have ''weak'' synchronization.

However, the global effect of the first transverse bifurcation (i.e., the fate of locally repelled trajectories through the first transverse bifurcation) depends on the existence of an absorbing area, controlling the global dynamics, inside the basin of attraction [8–10]. If there exists an absorbing area, acting as a bounded trapping vessel, locally repelled trajectories are restricted to move within the absorbing area, and exhibit intermittent bursting from the invariant subspace. For this case, the transverse Lyapunov exponent of the SCA is negative, and hence, the burst will tend to stop. However, in a real situation, noise of small intensity results in a continual sequence of intermittent bursts, called the attractor bubbling [11]. Thus, in the presence of an absorbing area, a bubbling transition occurs through the first transverse bifurcation. However, if such an absorbing area, enclosing the SCA, does not exist, the locally repelled trajectories will go to another attractor (or infinity). Consequently, the basin of attraction becomes riddled with a dense set of repelling tongues, belonging to the basin of another attractor (or infinity) [12], and hence, the SCA is no longer a topological attractor, because its basin does not contain any of its open neighborhood. However, it becomes a Milnor attractor in a measure-theoretical sense, because it attracts a set of initial conditions with positive Lebesgue measure [13]. Note that for this riddled case, a substantial improvement in the accuracy of the initial conditions yields only a small decrease in the uncertainty of the final state. Thus, in the absence of an absorbing area, a riddling transition takes place via the first transverse bifurcation.

With further variation of the coupling parameter, transversely stable periodic saddles embedded in the SCA are transformed into transversely unstable repellers due to successive transverse bifurcations, which intensify the bubbling and riddling effects. Eventually, the ''weights'' of the periodic saddles and repellers become balanced, and then a blow-out bifurcation occurs [14]. As a result of this blow-out transition, the SCA becomes transversely unstable (i.e., its transverse Lyapunov exponent becomes positive), and then complete desynchronization occurs. The global effect of this blow-out bifurcation also depends on the existence of an absorbing area. In the presence of the absorbing area, the blow-out bifurcation becomes gradual. Hence, a new asynchronous chaotic attractor, bounded to the absorbing area, appears through a supercritical (nonhysteric) blow-out bifurcation, and then it exhibits an intermittent bursting, called the on-off intermittency [15], where the long period of nearly synchronous state (off state) is occasionally interruppted by the short-time large-order burst (on state). However, without

*Electronic address: sykim@cc.kangwon.ac.kr

the absorbing area, an abrupt collapse of the synchronized state occurs through a subcritical (hysteric) blow-out bifurcation, and then typical trajectories starting near the invariant subspace are attracted to another distant attractor (or infinity).

For the study of chaos synchronization, two coupled identical one-dimensional (1D) maps, exhibiting period doublings, are usually used as a model. In this paper, we investigate the effect of the asymmetry of coupling on the loss of chaos synchronization in a system of two asymmetrically coupled 1D maps that contain a parameter α tuning the ''degree'' of asymmetry from the symmetric-coupling case ($\alpha=0$) [7] to the unidirectional-coupling case ($\alpha=1$) [10]. For many-coupled case, this kind of asymmetrically coupled maps are usually used to model open flow systems with preferred direction of propagation [16]. While increasing the asymmetry parameter α from 0 to 1, we investigate how the asymmetry affects the bifurcation mechanisms for the synchronization loss. It is thus found that the asymmetry changes the bifurcation scenarios for the desynchronization only when the symmetry-breaking pitchfork bifurcations are involved in the process of the loss of chaos synchronization for the symmetric-coupling case. In Sec. II, the bifurcation scenarios are investigated with the decreasing of the coupling parameter. For this weak-coupling case, pitchfork bifurcations of asynchronous periodic saddles are found to be replaced with saddle-node bifurcations. As the asymmetry parameter α is increased from 0, the type of the saddle-node bifurcations changes, and diverse effects occur. On the other hand, for the strong-coupling case, pitchfork bifurcations of synchronous periodic saddles are found to be transformed into the transcritical bifurcations in Sec. III. If such a transcritical bifurcation induces a contact of the SCA with its basin boundary, then a riddling transition occurs; otherwise, only a bubbling transition takes place. In such a way, the effect of the transcritical bifurcations also depends on their types. As a rule, the effects of the saddle-node and transcritical bifurcations for small α are similar to those of the pitchfork bifurcations in the symmetric-coupling case ($\alpha=0$) [7], although the underlying bifurcation mechanisms are different. However, with the further increasing of α, a significant change in the bifurcation effects occurs, and eventually the effects become similar to those in the unidirectionally coupled case ($\alpha=1$) [10]. Finally, a summary is given in Sec. IV.

II. BIFURCATION SCENARIOS FOR THE CASE OF WEAK COUPLING

In this section, with the decreasing of the coupling parameter, we investigate the effect of the asymmetry of coupling on the bifurcation scenarios of the loss of chaos synchronization. For this weak-coupling case, it is found that due to the asymmetry, subcritical pitchfork bifurcations of asynchronous periodic saddles are replaced by the saddle-node bifurcations, while other bifurcations, such as period-doubling bifurcations, are preserved. When the asymmetry parameter α is small, the bifurcation effect is similar to that for the symmetric-coupling case ($\alpha=0$). However, as α is increased, diverse bifurcation effects, that are different from those for $\alpha=0$, occur.

Let us consider two asymmetrically coupled identical 1D maps T,

$$T:\begin{cases} x_{t+1}=f(x_t)+(1-\alpha)c[f(y_t)-f(x_t)], \\ y_{t+1}=f(y_t)+c[f(x_t)-f(y_t)], \end{cases} \tag{1}$$

where x_t and y_t are state variables of the subsystems at a discrete time t, local dynamics in each subsystem is governed by the 1D map $f(x)=1-ax^2$, a is the control parameter of the 1D map, c is a coupling parameter, and α ($0\leqslant\alpha\leqslant 1$) is a parameter tuning the degree of asymmetry. The cases of $\alpha=0$ and 1 correspond to the symmetric and unidirectional couplings, respectively. Note that this asymmetrically coupled map T has an invariant synchronization line $y=x$, irrespectively of the symmetry. If an orbit lies on this synchronization line, then it is called a synchronous orbit; otherwise it is called an asynchronous orbit.

We also note that the coupled map T is noninvertible, because its Jacobian determinant $\det(DT)$ (DT is the Jacobian matrix of T) becomes zero along the critical curves, $L_0=\{(x,y)\in\mathbb{R}^2: x=0 \text{ or } y=0\}$. A finite number of segments of images L_k ($k=1,2,\ldots$) of the critical curves of L_0 can be used to define the boundary of an absorbing area $\mathcal{A}$ with the properties that (i) $\mathcal{A}$ is trapping (i.e., trajectories that enter $\mathcal{A}$ cannot leave it again) and (ii) superattracting (i.e., every point sufficiently close to the boundary of $\mathcal{A}$ will jump into $\mathcal{A}$ after a finite number of iterations) [17]. Furthermore, boundaries of an absorbing area can be also obtained by the union of segments of critical curves and portions of unstable manifolds of unstable periodic orbits. For this case, $\mathcal{A}$ is called a mixed absorbing area.

With increasing the control parameter a, the coupled map T exhibits an infinite sequence of period-doubling bifurcations of synchronous attractors with period 2^n ($n=0,1,2,\ldots$), ending at the accumulation point a_∞ ($=1.401\,155,\ldots$), in some region of c. This period-doubling cascade leads to creation of the SCA on the synchronization line. With further increase of a from a_∞, a sequence of band-merging bifurcations of the SCA take place. The set of a values yielding SCA's in the range $(a_\infty,2]$ forms a fat fractal with a positive Lebesgue measure, riddled with a dense set of windows of synchronous periodic attractors [18]. Hereafter, without loss of generality, we fix the value of a as $a=1.6$, where a single-band SCA exists on the synchronization line. Its transverse stability is determined by a transverse Lyapunov exponent,

$$\sigma_\perp=\ln|1-(2-\alpha)c|+\lim_{N\to\infty}\frac{1}{N}\sum_{t=1}^{N}\ln|2ax_t|. \tag{2}$$

For the symmetric-coupling case of $\alpha=0$, the following process of desynchronization was found [7]. As the coupling parameter c is decreased through $c=0.209,\ldots$, the saddle fixed point embedded in the SCA first becomes transversely unstable through a supercritical period-doubling bifurcation when its transverse Floquet (stability) multiplier,

$$\lambda_\perp=[1-(2-\alpha)c]f'(x^*) \tag{3}$$

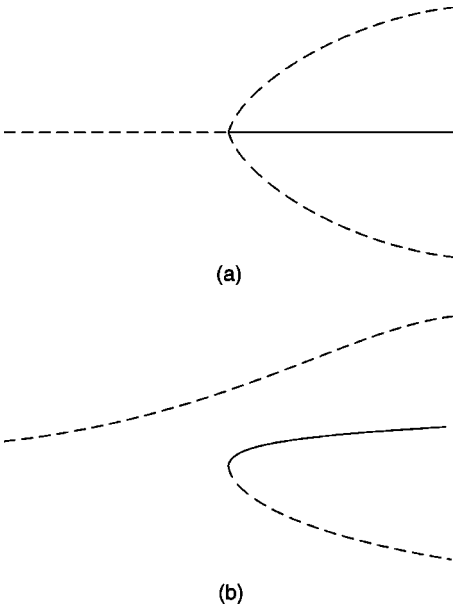

FIG. 1. Schematic bifurcation diagrams for (a) $\alpha=0$ and (b) $\alpha>0$ in the weak-coupling case. Here, the solid and dashed lines represent the periodic attractor and saddle, respectively. When the asymmetry is introduced (i.e., $\alpha\neq 0$), the (reverse) subcritical pitchfork bifurcation of an asynchronous periodic saddle for $\alpha=0$ is transformed into a smooth shift of the asynchronous periodic saddle (without any bifurcation) and a saddle-node bifurcation, creating a new pair of asynchronous saddle and stable node (attractor). For other details, see the text.

passes through -1, where x^* $[=(-1+\sqrt{1+4a})/2a]$ is the fixed point of the 1D map $f(x)$. After this first transverse bifurcation, the synchronous saddle fixed point is transformed into a repeller, and an asynchronous period-2 saddle appears in its vicinity. For this case, along with segments of the critical curves L_1 and L_2, portions of the unstable manifolds of the asynchronous period-2 saddle form a boundary of a mixed absorbing area, surrounding the SCA. Hence, locally repelled trajectories near the SCA cannot leave the mixed absorbing area, and they exhibit transient intermittent bursting from the synchronization line. Thus, this first transverse (period-doubling) bifurcation induces a bubbling transition. However, as c is further decreased, the asynchronous period-2 saddle becomes stabilized for $c=0.157,\ldots,$ through a (reverse) subcritical pitchfork bifurcation when its maximal Floquet (stability) multiplier decreases through $+1$ [see the schematic bifurcation diagram in Fig. 1(a)]. Then, the basin of the SCA becomes riddled with a dense set of repelling tongues leading to the asynchronous period-2 attractor. Note that this kind of stabilization of an asynchronous periodic saddle is the only mechanism of the riddling transition for the case of $\alpha=0$. With further decrease of the coupling parameter c, the SCA loses its transverse stability for $c\simeq 0.155$ through a blow-out bifurcation. After this subcritical blow-out bifurcation, the SCA transforms to a chaotic saddle with a positive transverse Lyapunov exponent, and the system is asymptotically attracted to the asynchronous period-2 attractor.

From now on, with increasing the asymmetry parameter from $\alpha=0$, we investigate the bifurcation scenarios of the loss of chaos synchronization. It is thus found that the asymmetry affects the bifurcation mechanism only for the case of the pitchfork bifurcation of an asynchronous periodic saddle, while other bifurcations such as period-doubling bifurcations are preserved. For the symmetric coupling case ($\alpha=0$), an asynchronous periodic saddle (denoted by the horizontal dashed line) is transformed into an attractor (denoted by the solid line) by emitting a pair of asynchronous saddles (denoted by the dashed lines) with the same period through a (reverse) subcritical pitchfork bifurcation, as shown in Fig. 1(a). However, as α is increased from $\alpha=0$, the upper-dashed branch for the case of $\alpha=0$ becomes split from the middle solid and lower-dashed branches. As a result, the asynchronous periodic saddle varies smoothly along the split upper branch without any bifurcation, and a pair of asynchronous saddle and stable node (attractor) appears along the former middle and lower branches via a saddle-node bifurcation, as shown in Fig. 1(b). In such a way, for small α the subcritical pitchfork bifurcation of an asynchronous periodic saddle is replaced with a saddle-node bifurcation, giving rise to the birth of a pair of new asynchronous saddle and stable node. However, as α is further increased, the type of the saddle-node bifurcation may be changed into another one, leading to the birth of a pair of new asynchronous saddle and unstable node (repeller), and then its effect becomes qualitatively different from that for $\alpha=0$, as will be seen below.

Figure 2 shows the phase diagram in the $\alpha-c$ plane. When passing the supercritical period-doubling bifurcation line D_1, the synchronous saddle fixed point first becomes transversely unstable, and an asynchronous period-2 saddle is born. After this first transverse bifurcation, the SCA is surrounded by a mixed absorbing area, acting as a bounded trapping vessel, and hence, locally repelled trajectories near the SCA exhibit transient intermittent bursting from the synchronization line. Thus, a bubbling transition occurs through the first transverse (period-doubling) bifurcation. Note that this period-doubling bifurcation mechanism for the bubbling transition and its effect are the same as those for $\alpha=0$, independently of the value of α. With further decrease of c, the SCA becomes transversely unstable through a blow-out bifurcation at the line B. However, the type of this blow-out bifurcation depends on the value of α. As mentioned above, with increasing α from 0, the subcritical pitchfork bifurction of the asynchronous period-2 saddle for $\alpha=0$ is replaced by the saddle-node bifurcation, which occurs on the heavy solid line S_2. As shown in the inset of Fig. 2, for $0<\alpha<\alpha_1$ $(\simeq 0.0078)$, a pair of asynchronous saddle and stable node with period 2 appears through the saddle-node bifurcation before the blow-out bifurcation. Consequently, the basin (shown in gray) of the SCA becomes riddled with a dense set of tongues, belonging to the basin (shown in dark gray) of the newly born asynchronous period-2 attractor (denoted by the solid circle), which is shown in Fig. 3 for $\alpha=0.005$ and $c=0.1555$. Note that the stable manifolds of the asynchronous period-2 saddles (denoted by the open circle and square) bound the main tongue, emanating from the synchronous repelling fixed point (denoted by the triangle). Here, an asynchronous period-2 saddle (square) is born from the syn-

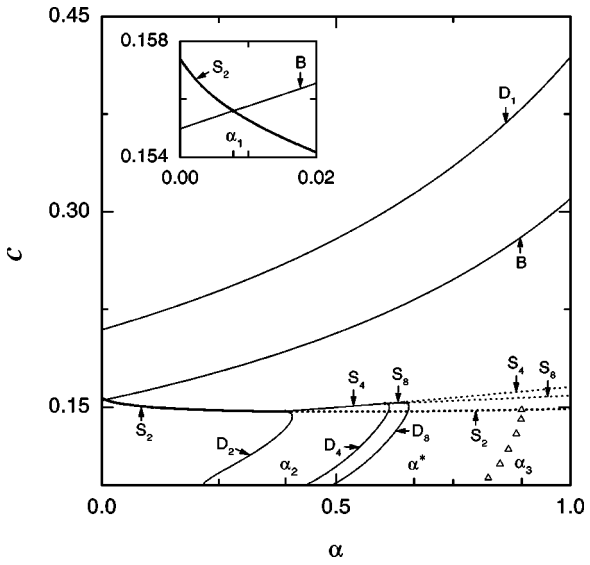

FIG. 2. Phase diagram in the $\alpha - c$ plane for the case of weak coupling. A bubbling transition occurs on the line D_1 through the supercritical period-doubling bifurcation of the saddle fixed point embedded in the SCA. With further decrease of c, the SCA becomes transversely unstable through a blow-out bifurcation on the line B. However, dynamical behaviors after the blow-out bifurcation vary depending on the value of α, particularly because of the diverse effect of the saddle-node bifurcation on the curve S_q ($q = 2^n$, $n = 1,2,\ldots$). The type of the saddle-node bifurcation on S_q changes at the point where the period-doubling bifurcation line D_q of an asynchronous period-q orbit touches the S_q line. Thus, a pair of asynchronous saddle and stable (unstable) node with period q appears when crossing the solid (dotted) part of S_q. Note also that an interior crisis occurs when the line, denoted by the triangles, is crossed. For other details, see the text.

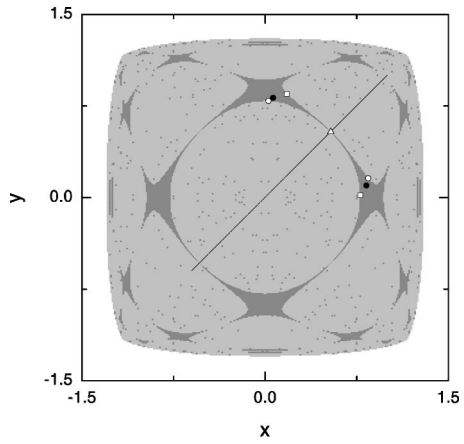

FIG. 3. Riddled basin of the SCA for $\alpha = 0.005$ and $c = 0.1555$ after the appearance of a new asynchronous period-2 attractor via a saddle-node bifurcation. Here, the square denotes an asynchronous period-2 saddle, born from the synchronous fixed point (denoted by the triangle), through the first transverse period-doubling bifurcation. A pair of asynchronous saddle (denoted by the open circle) and attractor (denoted by the solid circle) with period 2 appears through a saddle-node bifurcation. As a result, the basin of the SCA (shown in gray) becomes riddled with a dense set of tongues, belonging to the basin (shown in dark gray) of the asynchronous period-2 attractor.

chronous saddle fixed point (triangle) through the first transverse (period-doubling) bifurcation, while another asynchronous period-2 saddle (open circle) appears along with the asynchronous period-2 attractor (solid circle) via the saddle-node bifurcation. All the other tongues are preimages of this main tongue. Thus, the effect of the saddle-node bifurcation becomes the same as that of the subcritical pitchfork bifurcation for $\alpha = 0$ (i.e., a riddling transition occurs through the appearance of an asynchronous periodic attractor). For this case, when crossing the line B, the SCA loses its transverse stability via a subcritical blow-out bifurcation, and then the system is asymptotically attracted to the asynchronous period-2 attractor.

For $\alpha > \alpha_1$, the saddle-node bifurcation on S_2 occurs after the blow-out bifurcation (see the inset of Fig. 2). Hence, when passing the line B, an asynchronous chaotic attractor, bounded to the absorbing area, appears through a supercritical blow-out bifurcation and exhibits a typical intermittent bursting, called the on-off intermittency. However, the subsequent fate of the asynchronous chaotic attractor depends on the value of α. Figure 4(a) shows the asynchronous chaotic attractor for $\alpha = 0.2$ and $c = 0.15$, born via the supercritical blow-out bifurcation. However, when passing the S_2 line, the asynchronous chaotic attractor becomes broken up suddenly, because a pair of asynchronous saddle and stable node (attractor) with period 2 appears inside the asynchronous chaotic attractor via the saddle-node bifurcation. After this break up, the asymptotic state changes from the asynchronous chaotic state to an asynchronous period-2 state (denoted by the solid circle), as shown in Fig. 4(b) for $\alpha = 0.2$ and $c = 0.14$, where an open circle denotes an asynchronous period-2 saddle born via the saddle-node bifurcation. Note that this destruction effect of the saddle-node bifurcation is in contrast with the riddling effect for $\alpha < \alpha_1$. This kind of destruction through the appearance of an asynchrnous period-2 attractor occurs only when passing the heavy solid part of the S_2 curve for $\alpha_1 < \alpha < \alpha_2$ ($\simeq 0.3924$) (see Fig. 2). Note that for $\alpha = \alpha_2$, a period-doubling bifurcation line D_2 of an asynchronous period-2 orbit touches the saddle-node bifurcation line S_2, and then the type of the saddle-node bifurcation changes from the unstable-stable pair bifurcation to the unstable-unstable pair bifurcation. That is, when passing the heavy dotted part of the S_2 curve for $\alpha > \alpha_2$, a pair of asynchronous saddle and unstable node (repeller) with period 2 appears. We also note that a saddle-node bifurcation line S_4, giving rise to the birth of a pair of asynchronous saddle and stable node with period 4, emanates from the contact point of the S_2 line with the D_2 line. In such a way, with increasing α higher-order saddle-node and period-doubling bifurcations of period-q ($q = 2^n$, $n = 2,3,4,\ldots$) orbit occur on the S_q and D_q curves, respectively. Thus, the destruction of the asynchronous chaotic attractor continues to take place through the appearance of an asynchronous period-q attractor when passing the solid part of the S_q curve until $\alpha = \alpha^*$ ($\simeq 0.6673$) (see Fig. 2). For $\alpha > \alpha^*$, the type of all saddle-node bifurcations on the S_q curves becomes the unstable-unstable pair bifurcations, giving rise to the birth of

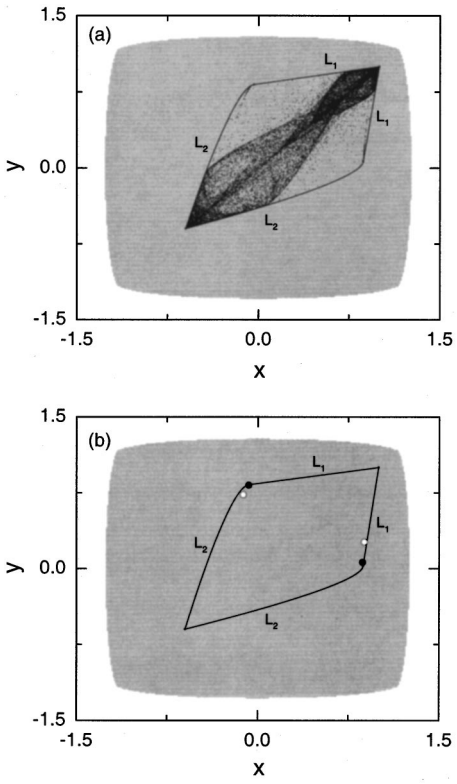

FIG. 4. Destruction of an asynchronous chaotic attractor through the appearance of an asynchronous period-2 attractor inside the asynchronous chaotic attractor via a saddle-node bifurcation for $\alpha = 0.2$. (a) The asynchronous chaotic attractor bounded by segments of the critical curves L_1 and L_2 for $c = 0.15$, born via a supercritical blow-out bifurcation. (b) Asynchronous period-2 attractor (denoted by the solid circle) and its counterpart saddle (denoted by the open circle) for $c = 0.14$ after the destruction of the asynchronous chaotic attractor.

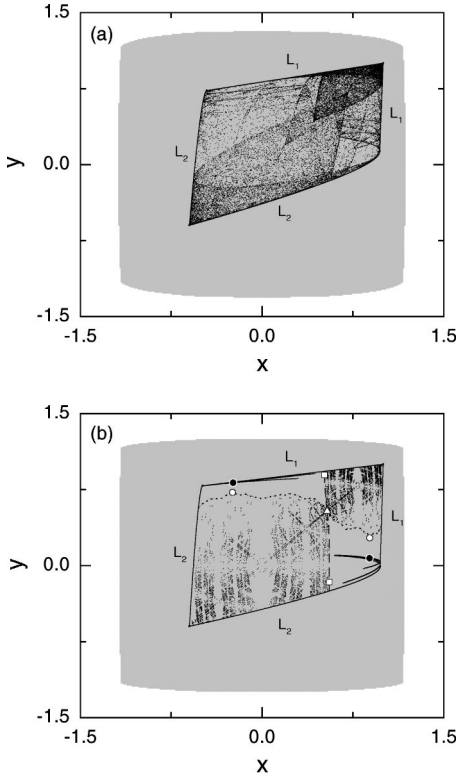

FIG. 5. Appearance of a small asynchronous chaotic attractor through a (reverse) interior crisis for $\alpha = 0.85$. (a) Large asynchronous chaotic attractor bounded by the segments of the critical curves L_1 and L_2 for $c = 0.18$, born via a supercritical blow-out bifurcation. (b) Small asynchronous chaotic attractor for $c = 0.14$ born through a (reverse) interior crisis, mediated by a saddle-node bifurcation on S_2. Note that the dotted and dashed lines bound the region, where unstable asynchronous periodic orbits lie inside the absorbing area bounded by segments of the critical curves L_1 and L_2. Here, unstable asynchronous orbit points are plotted up to period 16. The asynchronous period-2 saddle (denoted by the solid circle) is embedded in the asynchronous chaotic attractor and the asynchronous period-2 repeller (denoted by the open circle) lies on the dotted line. As c is further decreased, this asynchronous small chaotic attractor is transformed into a large one through another interior crisis occurring when crossing the dashed line, where the asynchronous period-2 orbit (denoted by the square), born through the first transverse period-doubling bifurcation of the synchronous fixed point (represented by the triangle) lies. For other details, see the text.

asynchronous saddle-repeller pairs, and hence, destruction phenomena no longer occur.

For $\alpha > \alpha^*$, a large asynchronous chaotic attractor, born via the blow-out bifurcation, is transformed into a small chaotic attractor through a reverse interior crisis, mediated by the saddle-node bifurcation. Figure 5(a) shows the large asynchronous chaotic attractor, bounded by the segments of the critical curves L_1 and L_2 for $\alpha = 0.85$ and $c = 0.18$. When passing the dotted S_2 curve for $c \simeq 0.1476$, along with a pair of asynchronous saddle and repeller with period 2, born through the saddle-node bifurcation, a small two-piece asynchronous chaotic attractor appears, as shown in Fig. 5(b) for $c = 0.14$. Note that the asynchronous period-2 saddle (denoted by the solid circle) is embedded in the small asynchronous chaotic attractor, and the asynchronous period-2 repeller (denoted by the open circle) lies on the dotted line. In fact, all higher-order asynchronous period-q saddles and repellers, born via the saddle-node bifurcations on S_q, also lie on the asynchronous chaotic attractor and the dotted line, respectively. On the other hand, the asynchronous period-2 orbit (denoted by the square), born via the first transverse period-doubling bifurcation of the synchronous fixed point (denoted by the triangle), and its descendant orbits lie on the dashed line. Note that these two lines are bounding a region, where asynchronous unstable periodic orbits (denoted by dots) lie, inside the absorbing area. As we increase the coupling parameter c from 0.14 in a reverse way, the asynchronous period-2 saddle (solid circle) on the asynchronous chaotic attractor approaches the asynchronous period-2 repeller (open circle) on the dotted boundary line, and they coalesce at their saddle-node bifurcation point ($c \simeq 0.1476$) on S_2. After that, a sudden increase in the size of the asynchronous chaotic attractor occurs through the interior crisis mediated by the saddle-node bifurcation. A similar expansion of the asynchronous chaotic attractor also takes place through another interior crisis when decreasing the coupling parameter

c from 0.14. With the decrease of c, the asynchronous chaotic attractor becomes larger in a horizontal direction, and it collides with the dashed boundary line when passing the crisis line, denoted by the triangles in Fig. 2. After that, the small asynchronous chaotic attractor transforms to a large asynchronous chaotic attractor, covering the whole absorbing area. Note that this interior-crisis curve touches the S_2 curve for $\alpha=\alpha_3$ ($\simeq 0.8965$) (see Fig. 2). Hence, for $\alpha>\alpha_3$, no interior crises occur when passing the S_2 curve. Consequently, the large asynchronous chaotic attractor, born via the blow-out bifurcation, is preserved without any qualitative change when passing the S_2 curve, as in the unidirectionally coupled case ($\alpha=1$) [10].

III. BIFURCATION SCENARIOS FOR THE CASE OF STRONG COUPLING

In this section, we investigate the effect of the asymmetry of coupling on the bifurcation scenarios of desynchronization with increasing the coupling parameter. For this strong-coupling case, it is found that the asymmetry changes the supercritical pitchfork bifurcation of a synchronous periodic saddle into a transcritical bifurcation. However, the effect of the transcritical bifurcation varies depending on whether or not it induces a contact between the SCA and its basin boundary. If such a contact does not occur, a bubbling transition occurs, while when a contact is induced, a riddling transition takes place. For small α, the transcritical bifurcation does not induce any contact, and hence, its effect becomes similar to that in the symmetrically coupled case ($\alpha=0$). However, as α is further increased, the type of the transcritical bifurcation is changed into another one inducing a contact, and then the effect of the transcritical bifurcation becomes qualitatively different from that for $\alpha=0$.

For the case of the symmetric coupling ($\alpha=0$), the following desynchronization process was found [7]. The synchronous saddle fixed point embedded in the SCA first becomes transversely unstable via a supercritical pitchfork bifurcation when its minimal Floquet multiplier increases through $+1$ for $c=0.790,\ldots$. As a result of this first transverse bifurcation, the synchronous saddle fixed point is transformed into a repelling fixed point, and a conjugate pair of asynchronous period-1 saddle appears in its neighborhood [see the schematic bifurcation diagram in Fig. 6(a)]. For this case, the SCA is surrounded by a mixed absorbing area, bounded by union of segments of the unstable manifolds of the asynchronous period-1 saddle and portions of the critical curves L_1 and L_2. Hence, locally repelled trajectories near the SCA cannot leave the mixed absorbing area, and they exhibit transient intermittent bursting. Thus, the first transverse (pitchfork) bifurcation induces a bubbling transition. With further increase of c, the asynchronous period-1 saddles are stabilized through subcritical period-doubling bifurcations for $c=0.842,\ldots$. Consequently, the basin of the SCA becomes riddled with a dense set of tongues, belonging to the basins of the stabilized asynchronous period-1 attractors. This riddling transition is similar to the weak-coupling case for $\alpha=0$, although the underlying bifurcation mechanisms for the stabilization are different. As c is further increased, the SCA becomes transversely unstable through a subcritical blow-out bifurcation for $c\simeq 0.845$, and then the system is asymptotically attracted to one of the asynchronous period-1 attractors.

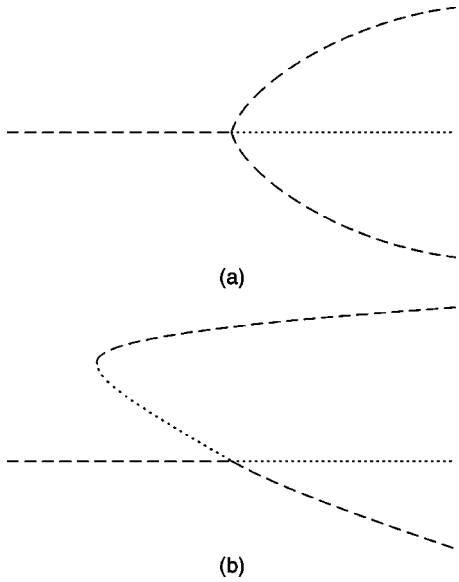

FIG. 6. Schematic bifurcation diagrams for (a) $\alpha=0$ and (b) $\alpha>0$ in the strong-coupling case. Here, the dashed and dotted lines represent the periodic saddle and repeller, respectively. When the asymmetry is introduced (i.e., $\alpha\neq 0$), the supercritical pitchfork bifurcation of a synchronous periodic saddle for $\alpha=0$ is transformed into a transcritical bifurcation of the synchronous periodic saddle and a saddle-node bifurcation, creating a new pair of asynchronous saddle and unstable node (repeller). For other details, see the text.

We now investigate the bifurcation scenarios of the synchronization loss with increasing the asymmetry parameter from $\alpha=0$. It is thus found that the bifurcation mechanism for the case of the pitchfork bifurcation of a synchronous periodic saddle is affected by the asymmetry, while other bifurcations such as period-doubling bifurcations are conserved. For the symmetric coupling case ($\alpha=0$), a synchronous periodic saddle (denoted by the horizontal dashed line) is transformed into a repeller (denoted by the dotted line) by emitting a conjugate pair of asynchronous saddles (denoted by the dashed lines) with the same period through a supercritical pitchfork bifurcation, as shown in Fig. 6(a). However, with increasing the asymmetry parameter from $\alpha=0$, the upper branch for the case of $\alpha=0$ is smoothly shifted backward from the bifurcation point, and then two new branches, corresponding to the asynchronous periodic saddle (dashed line) and repeller (dotted line), appear through a saddle-node bifurcation, as shown in Fig. 6(b). Note that with increasing the coupling parameter, the asynchronous periodic repeller (dotted line) approaches the synchronous periodic saddle (horizontal dashed line), and eventually they coalesce at a bifurcation point. After that, they exchange only their stability [i.e., the saddle (repeller) transforms to a repeller (saddle)]. Through this transcritical bifurcation, occurring in asymmetric dynamical systems with some constraint [19], the synchronous periodic saddle loses its trans-

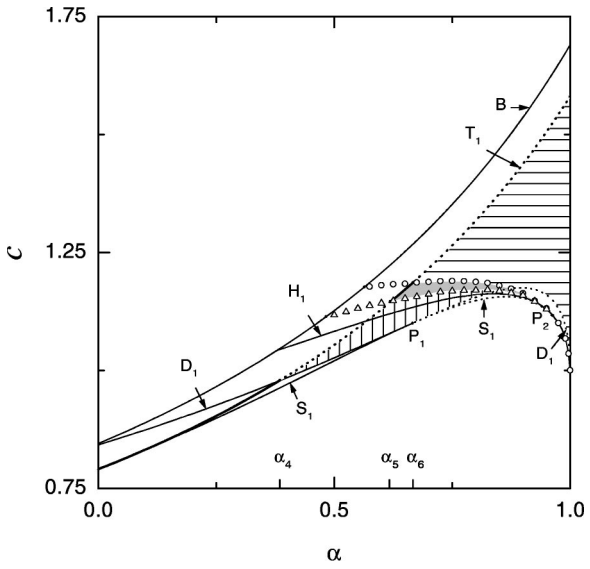

FIG. 7. Phase diagram before the blow-out bifurcation in the $\alpha-c$ plane for the strong-coupling case. The synchronous saddle fixed point first becomes transversely unstable through a transcritical bifurcation on the line T_1. The effect of the transcritical bifurcation varies depending on whether or not it induces a contact between the SCA and its basin boundary. An asynchronous period-1 repeller, which is a counterpart of the synchronous period-1 saddle for the transcritical bifurcation, lies on a basin boundary of the SCA in the regions hatched with vertical and horizontal lines. Hence, when crossing the dotted part of T_1, a riddling transition through the transcritical contact bifurcation occurs, while when its solid part is crossed, a bubbling transition takes place, because an absorbing area surrounding the SCA is preserved. Thus, the T_1 curve is divided into four parts (two heavy solid parts and two heavy dotted parts). Other diverse dynamical phenomena also occur on the saddle-node bifurcation curve S_1, period-doubling bifurcation curve D_1, Hopf bifurcation curve H_1, boundary-crisis curves (denoted by the open triangles and circles), and blow-out bifurcation curve B. For further details, see the text.

verse stability, when its minimal Floquet multiplier increases through $+1$. However, the effect of this transcritical bifurcation depends on whether or not it induces a contact between the SCA and its basin boundary, as will be seen below.

Figure 7 shows the phase diagram before the blow-out bifurcation in the $\alpha-c$ plane. As mentioned above, for $\alpha>0$ the synchronous saddle fixed point first becomes transversely unstable through a transcritical bifurcation, occurring on the line T_1, where the synchronous saddle fixed point exchanges stability with an asynchronous repelling fixed point, born through a saddle-node bifurcation occurring on the line S_1. Note that these transcritical and saddle-node bifurcation lines T_1 and S_1 emanate from the pitchfork bifurcation point for $\alpha=0$. The type of the transcritical bifurcation of the synchronous saddle fixed point depends on whether or not its ''counterpart'' (asynchronous repelling fixed point) lies on a basin boundary. Note that the asynchronous period-1 repeller is lying on a basin boundary in the regions hatched with vertical and horizontal lines. Only when the synchronous period-1 saddle collides with an asynchronous period-1 repeller on a basin boundary, the transcritical bifurcation may induce a contact between the SCA and its basin boundary, and then an absorbing area, surrounding the SCA, disappears. Consequently, when crossing the heavy dotted part of the T_1 curve, a direct transition to riddling occurs, while when its heavy solid part is passed, a bubbling transition takes place because an absorbing area, surrounding the SCA, is preserved. Thus, the T_1 curve is divided into four parts (two heavy solid parts and two heavy dotted parts). The values of α at their boundary points are α_4 ($\simeq 0.3846$), α_5 ($\simeq 0.6187$), and α_6 ($\simeq 0.6667$).

For $0<\alpha<\alpha_4$, when crossing the S_1 curve, a pair of asynchronous period-1 saddle (denoted by the solid down triangle) and unstable node (repeller, denoted by the open down triangle) appears, as shown in Fig. 8(a) for $\alpha=0.3$ and $c=0.923$. Together, with segments of the critical curves L_1 and L_2, portions of the unstable manifolds of the asynchronous saddle fixed point (solid down triangle) form a boundary of a mixed absorbing area, surrounding the SCA. Note that the asynchronous period-1 repeller (open down triangle) lies strictly inside the absorbing area (i.e., it does not lie on any basin boundary). As c is increased, the asynchronous period-1 repeller (open down triangle) approaches the synchronous period-1 saddle (denoted by the open up triangle), embedded in the SCA. Eventually, they coalesce and a transcritical bifurcation occurs for $c=0.930,\ldots$. When passing the transcritical bifurcation point, the asynchronous period-1 repeller (open down triangle) moves down off the synchronization line, and exchanges stability with the synchronous period-1 saddle (open up triangle), as shown in Fig. 8(b) for $c=0.943$. Since the mixed absorbing area is still surrounding the SCA, locally repelled trajectories near the SCA exhibit transient intermittent bursting from the synchronization line. Thus, the effect of the transcritical bifurcation becomes similar to that of the supercritical pitchfork bifurcation for $\alpha=0$ (i.e., a bubbling transition occurs). With further increase of c, the asynchronous saddle fixed point becomes stabilized through a subcritical period-doubling bifurcation when crossing the D_1 line for $c=0.945,\ldots$. Consequently, the basin (shown in gray) of the SCA becomes riddled with a dense set of tongues, belonging to the basin (shown in dark gray) of the stabilized asynchronous period-1 attractor (solid down triangle), which is shown in Fig. 8(c) for $c=0.992$. Note that this stabilization mechanism is the same as that for $\alpha=0$.

When α increases through α_4, the D_1 curve crosses the T_1 curve (see Fig. 7). Consequently, for $\alpha>\alpha_4$ the stabilization of the asynchronous period-1 saddle (solid down triangle) through a subcritical period-doubling bifurcation occurs before the first transverse (transcritical) bifurcation on the T_1 curve. As a result of this stabilization, the asynchronous period-1 repeller (open down triangle) lies on the basin (shown in dark gray) boundary of the stabilized asynchronous period-1 attractor (solid down triangle), as shown in Fig. 9(a) for $\alpha=0.48$ and $c=1.03$. For this case, a mixed absorbing area, formed by the union of segments of the unstable manifolds of the asynchronous period-1 repeller and portions of the critical curves L_1 and L_2, is surrounding the SCA. As c is increased, the asynchronous period-1 repeller

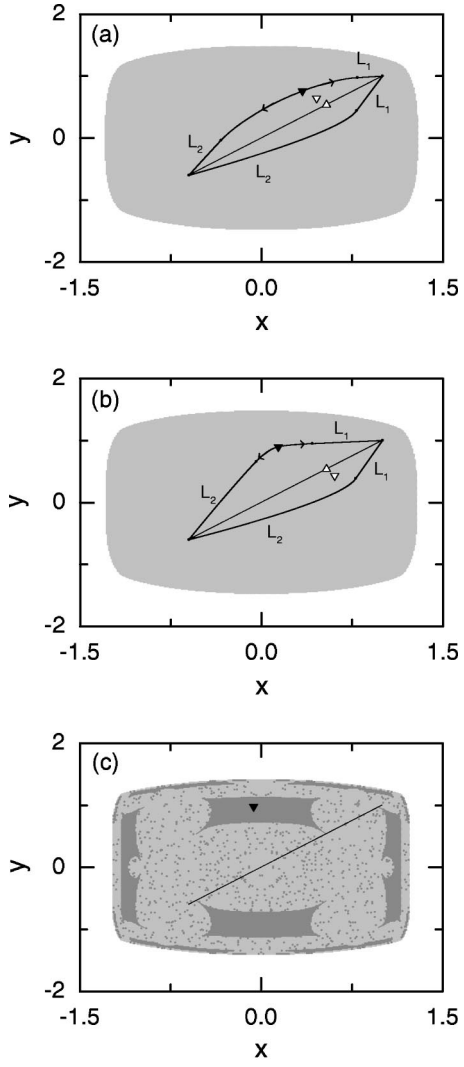

FIG. 8. Bubbling transition through the transcritical bifurcation that does not induce any contact between the SCA and its basin boundary for $\alpha = 0.3$. Here, the asynchronous period-1 saddle and repeller, born through the saddle-node bifurcation on S_1, are denoted by the solid and open down triangles, respectively, and the synchronous period-1 saddle is represented by the open up triangle. The situations before and just after the transcritical bifurcation of the synchronous period-1 saddle are depicted in (a) for $c = 0.923$ and in (b) for $c = 0.943$, respectively. (c) Basin (shown in gray) of the SCA for $c = 0.992$, riddled with a dense set of tongues, belonging to the basin (shown in dark gray) of the stabilized asynchronous period-1 attractor (solid down triangle), through a subcritical period-doubling bifurcation.

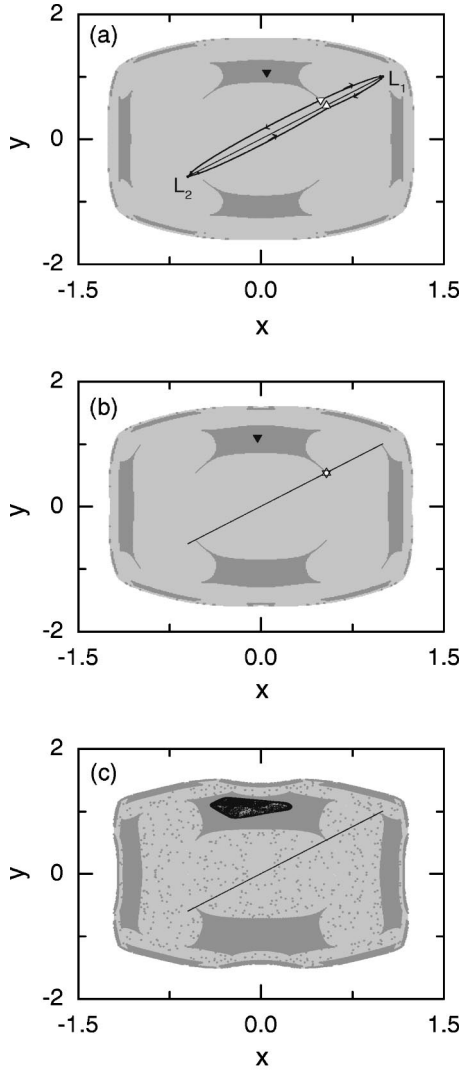

FIG. 9. Riddling transition through the transcritical contact bifurcation for $\alpha = 0.48$. Before the transcritical bifurcation, the asynchronous period-1 saddle (denoted by the solid down triangle) becomes stabilized through a subcritical period-doubling bifurcation, and hence, the asynchronous period-1 repeller (denoted by the open down triangle), which is the counterpart of the synchronous period-1 saddle (represented by the open up triangle) lies on the basin boundary. The situations before and just at the transcritical bifurcation of the synchronous period-1 saddle are depicted in (a) for $c = 1.03$ and in (b) for $c = 1.040\ldots,$, respectively. (c) Basin (shown in gray) of the SCA for $c = 1.1$, riddled with a dense set of tongues, belonging to the basin (shown in dark gray) of the asynchronous chaotic attractor, developed from the asynchronous period-1 attractor (solid down triangle).

(open down-triangle) approaches the synchronous period-1 saddle (open up-triangle), embedded in the SCA, and hence, the absorbing area shrinks. Eventually, for $c = 1.040, \ldots,$ a transcritical contact bifurcation between the synchronous period-1 saddle and the asynchronous period-1 repeller on the basin boundary occurs, and then the absorbing area disappear, as shown in Fig. 9(b). Note that this transcritical bifurcation induces a contact between the SCA and its basin boundary. When passing the transcritical bifurcation point, the asynchronous period-1 repeller (open down triangle) moves down off the basin boundary, and exchanges stability with the synchronous period-1 saddle (open up triangle). However, the SCA continues to contact its basin boundary at a new synchronous repelling fixed point (open up triangle). As a result of this transcritical bifurcation, the basin of the SCA becomes riddled with a dense set of tongues, belonging to the basin of the asynchronous period-1 attractor (solid down triangle). Thus, this transcritical bifurcation induces a riddling transition. However, near the riddling transition

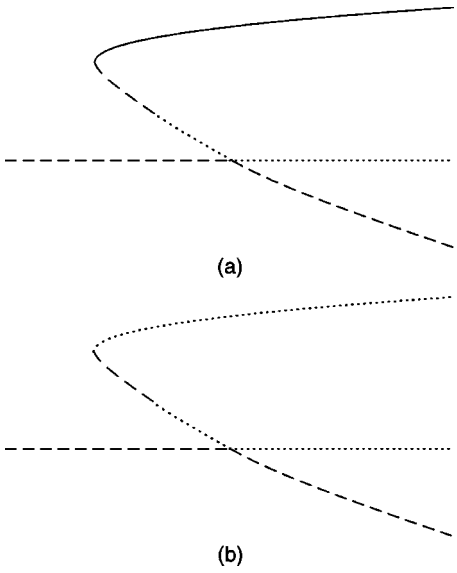

FIG. 10. Types of the saddle-node bifurcation, associated with the transcritical bifurcation, for large α (>0.666). Solid, dashed, and dotted lines denote the attractor, saddle, and repeller, respectively. The saddle-node bifurcation gives rise to the birth of a pair of asynchronous saddle and (a) stable or (b) unstable node. For both cases, the asynchronous saddle is transformed into a repeller, acting as the counterpart of the synchronous saddle for the transcritical bifurcation, through a period-doubling bifurcation.

point, the tongues are too narrow to be seen. With further increase of c, the asynchronous period-1 attractor (solid down triangle) is transformed into a quasiperiodic attractor through a Hopf bifurcation when crossing the H_1 curve, and then an asynchronous chaotic attractor is developed from the quasiperiodic attractor. During this process, the repelling tongues become large to be seen, as shown in Fig. 9(c) for $c=1.1$. Note that this kind of a direct transition to riddling takes place when passing the heavy dotted part of the T_1 curve for $\alpha_4<\alpha<\alpha_5$, in contrast to the case of $\alpha<\alpha_4$ where only a bubbling transition occurs through the transcritical bifurcation on T_1.

As α is increased from α_5, the D_1 curve touches the S_1 curve at the point P_1 [$\simeq(0.6660,1.0999)$], and then the type of the saddle-node bifurcation changes (see Fig. 7). On the solid part of S_1 (below P_1), the saddle-node bifurcation gives rise to the birth of a pair of asynchronous period-1 saddle and unstable node (repeller), while on the dotted part of S_1 (above P_1), it leads to the birth of a pair of asynchronous period-1 saddle and stable node (attractor) [see the schematic bifurcation diagram in Fig. 10(a)]. Note also that a supercritical period-doubling bifurcation (dotted) line D_1 emanates from P_1, in contrast with the subcritical solid part of D_1 below P_1. At the right end point P_2 [$\simeq(0.9635,1.1161)$] of the dotted part of S_1, where the curve H_1 touches the curve S_1, the type of the saddle-node bifurcation changes again, i.e., on the solid part of S_1 above P_2, a pair of asynchronous period-1 saddle and unstable node (repeller) is born [see also the schematic bifurcation diagram in Fig. 10(b)]. As shown in Figs. 10(a) and (b), for $\alpha>0.666$ (above P_1) the asynchronous period-1 saddle,

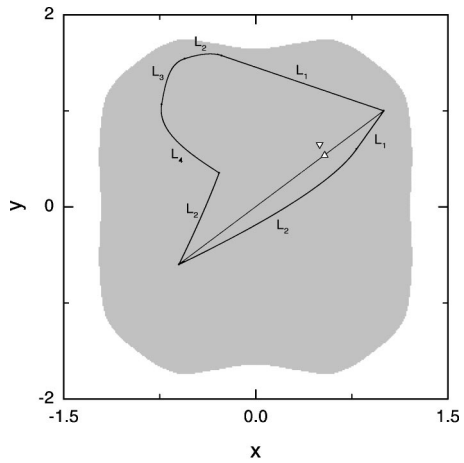

FIG. 11. SCA surrounded by a large absorbing area for $\alpha=0.68$ and $c=1.17$. Note that the asynchronous period-1 repeller (denoted by the open down triangle), which acts as the counterpart of the synchronous period-1 saddle (denoted by the open up triangle) for the transcritical bifurcation, lies strictly inside the absorbing area.

born through a saddle-node bifurcation, is transformed into a repeller via a supercritical period-doubling bifurcation, which then becomes a counterpart of the synchronous period-1 saddle for the transcritical bifurcation. This is in contrast to the case of $\alpha<0.666$ (below P_1), where the asynchronous period-1 repeller, born through a saddle-node bifurcation, is involved in the transcritical bifurcation as a counterpart of the synchronous period-1 saddle.

The asynchronous period-1 repellers, associated with the transcritical bifurcations, lie on the basin boundary of an asynchronous period-1 attractor (or an attractor developed from it) in the region hatched with vertical lines in Fig. 7. Here, the asynchronous period-1 attractor appears through stabilization of the asynchronous period-1 saddle born through the saddle-node bifurcation for $\alpha<0.666$, while for $\alpha>0.666$, it is just the attractor born through the saddle-node bifurcation on the dotted part of S_1. For this case, the SCA is surrounded by a small mixed absorbing area [e.g., see Fig. 9(a)]. For $\alpha>\alpha_5$, the asynchronous chaotic attractor developed from the asynchronous period-1 attractor disappears with its basin through a boundary crisis when crossing the line denoted by the open triangles in Fig. 7. Note that this boundary-crisis curve ends at the point P_2. Thus, when entering the shaded region through the boundary-crisis curve, the whole basin becomes occupied only by the SCA, surrounded by a large absorbing area, which is shown in Fig. 11 for $\alpha=0.68$ and $c=1.17$. Note that the asynchronous period-1 repeller [open down triangle: counterpart of the synchronous period-1 saddle (open up triangle) for the transcritical bifurcation] lies strictly inside the absorbing area (i.e., it no longer lies on any basin boundary). Hence, when passing the solid part of T_1 for $\alpha_5<\alpha<\alpha_6$ (left boundary of the shaded region), the transcritical bifurcation does not induce any contact between the SCA and its basin boundary. After this transcritical bifurcation, locally repelled trajectories near the SCA exhibit transient intermittent bursting from the synchronization line (i.e., a bubbling transition occurs),

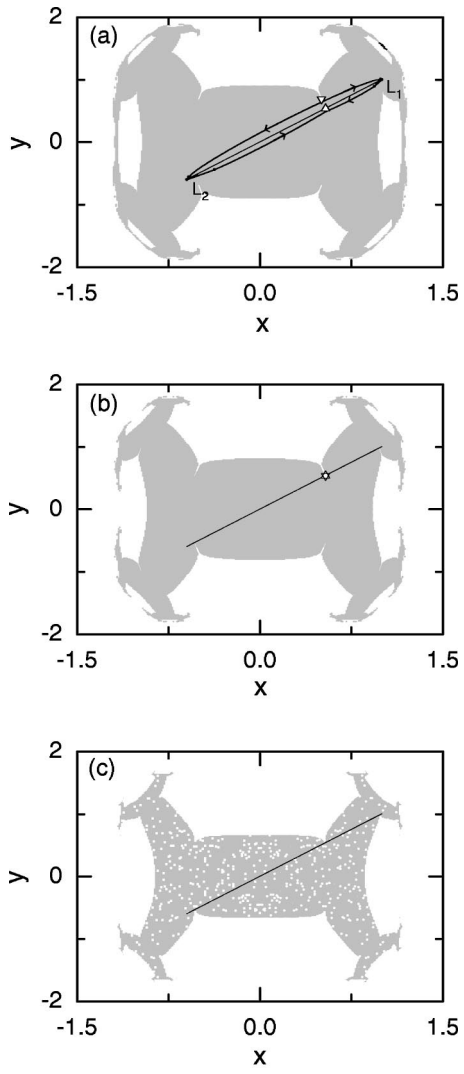

FIG. 12. Riddling transition through the transcritical contact bifurcation for $\alpha=0.8$. (a) SCA surrounded by a mixed absorbing area for $c=1.27$. Note that the asynchronous period-1 repeller (denoted by the open down triangle), which is the counterpart of the synchronous period-1 saddle (represented by the open up triangle), lies on the basin boundary. (b) At the transcritical bifurcation point ($c=1.317,\ldots$), the saddle (open up triangle) and the repeller (open down triangle) coalesce, and thus, the absorbing area disappears. (c) Basin (shown in gray) of the SCA for $c=1.4$, riddled with a dense set of tongues, belonging to the basin (shown in white) of the attractor at infinity.

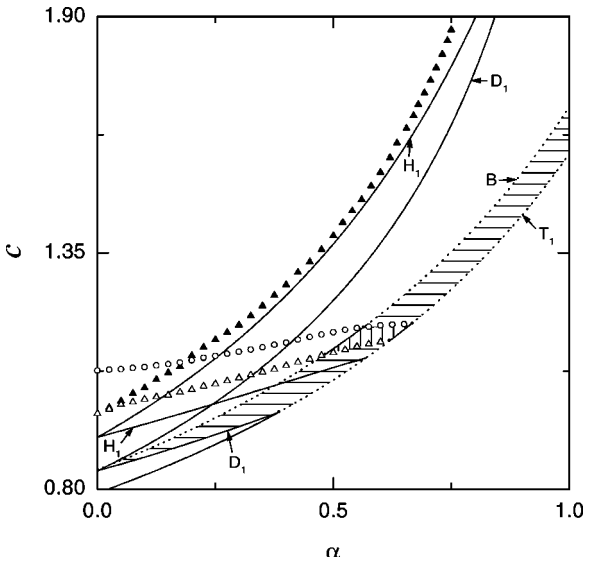

FIG. 13. Phase diagram after the transcritical bifurcation in the $\alpha-c$ plane for the case of strong coupling. As a result of the transcritical bifurcation at the line T_1, a riddling transition occurs in the horizontally-hatched region, while a bubbling transition takes place in the vertically hatched region. Hence, when crossing the dotted and solid parts of the curve *B*, subcritical and supercritical blow-out bifurcations occur, respectively. Note also that the period-doubling bifurcation curves D_1, the Hopf bifurcation curves H_1, and the boundary-crisis curves (denoted by the open and solid triangles) come in pairs from the period-doubling bifurcation, Hopf bifurcation, and the crisis points for $\alpha=0$, respectively. For further details, see the text.

because the large absorbing area, surrounding the SCA, is preserved.

However, when crossing the upper boundary of the the shaded region, denoted by the open circles in Fig. 7, the large absorbing area disappears suddenly through a contact with the basin boundary of the SCA. As a result of this crisis of the absorbing area, the basin (shown in white) of the attractor at infinity penetrates the basin (shown in gray) of the SCA, as shown in Fig. 12(a) for $\alpha=0.8$ and $c=1.27$. Note that the asynchronous period-1 repeller [open down triangle: counterpart of the synchronous period-1 saddle (open up triangle) for the transcritical bifurcation] lies on the basin boundary of the SCA, surrounded by a small mixed absorbing area. This kind of situation occurs in the whole region hatched with horizontal lines in Fig. 7. With the increasing of the coupling parameter *c*, the asynchronous period-1 repeller (open down triangle) approaches the synchronous period-1 saddle (open up triangle), the mixed absorbing area shrinks, and eventually a transcritical contact bifurcation occurs when crossing the upper dotted part of T_1 for $c=1.317,\ldots,$ as shown in Fig. 12(b). As a result of this transcritical bifurcation, the basin of the SCA becomes riddled with a dense set of repelling tongues, leading to the divergent trajectories, because the mixed absorbing area, surrounding the SCA, disappears, which is shown in Fig. 12(c) for $c=1.4$. Note that this mechanism for the riddling transition through the transcritical contact bifurcation on the upper dotted part of T_1 is similar to that in the unidirectionally-coupled case ($\alpha=1$) [10].

From now on, we study the dynamical behaviors after the bubbling and riddling transitions. Figure 13 shows the phase diagram after the transcritical bifurcation in the α-c plane. As explained above, a direct transition to riddling occurs through a transcritical contact bifurcation when crossing the dotted part of T_1, because the absorbing area, surrounding the SCA, disappears. On the other hand, when the solid part of T_1 is crossed, a bubbling transition takes place, because an absorbing area is surrounding the SCA. However, with further increase of *c*, a riddling transition also occurs through stabilization of an asynchronous period-1 saddle, born by the

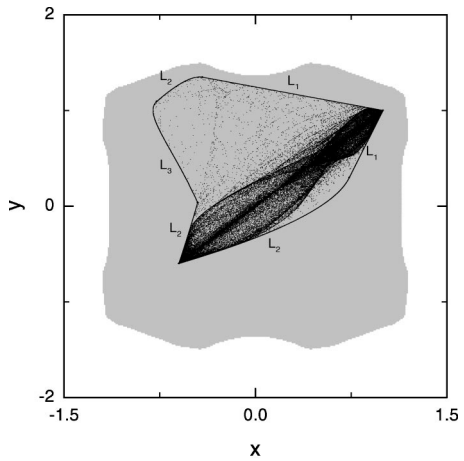

FIG. 14. Large asynchronous chaotic attractor, born via a supercritical blow-out bifurcation for $\alpha=0.5$ and $c=1.14$, which covers the whole absorbing area, bounded by the segments of the critical curves, L_1, L_2, and L_3.

saddle-node bifurcation on S_1, via a subcritical period-doubling bifurcation on the lower branch of D_1. Thus, the basin of the SCA becomes riddled in the region hatched with horizontal lines, while an absorbing area is surrounding the SCA in the region hatched with vertical lines. Eventually, when crossing the blow-out bifurcation curve *B*, the SCA becomes transversely unstable, and then it is transformed into a chaotic saddle (i.e., a complete loss of chaos synchronization occurs). However, the type of the blow-out bifurcation also depends on the existence of an absorbing area. When crossing the lower- and upper-dotted parts of *B*, the state of the system is asymptotically attracted to an asynchronous period-1 attractor (or an asynchronous attractor developed from it) and the attractor at infinity, respectively, through a subcritical blow-out bifurcation, because there is no absorbing area. Note also that the blow-out bifurcations near $\alpha=0$ and 1 are similar to those in the cases of symmetric coupling ($\alpha=0$) [7] and unidirectional coupling ($\alpha=1$) [10], respectively. However, when crossing the solid part of *B*, an asynchronous chaotic attractor spreads to the whole absorbing area through a supercritical blow-out bifurcation, as shown in Fig. 14 for $\alpha=0.5$ and $c=1.14$. This asynchronous chaotic attractor makes a contact with its basin boundary on the curve, denoted by the open circles in Fig. 13, and then it disappears with its basin through a boundary crisis.

Finally, we discuss the bifurcation behaviors after the blow-out bifurcation. As shown in Fig. 13, as α is increased from 0, the period-doubling bifurcation curves D_1, the Hopf bifurcation curves H_1, and the boundary-crisis curves (denoted by the open and solid triangles) come in pairs from the period-doubling bifurcation, Hopf bifurcation, and the crisis points for $\alpha=0$, respectively. For the case of subcritical period-doubling bifurcations on D_1, the lower branch of D_1 is associated with stabilization of the asynchronous period-1 saddle [corresponding to the upper-dashed curve in Fig. 6(b)], born through the saddle-node bifurcation. On the other hand, when crossing the upper branch of D_1 another period-1 saddle [corresponding to the lower-dashed curve in Fig. 6(b)], which is transformed from the asynchronous period-1 repeller through the transcritical bifurcation in Fig. 6(b), also becomes stabilized. These asynchronous period-1 attractors, stabilized at the upper and lower branches of D_1, become unstable when passing the upper and lower branches of H_1, respectively, and then generally quasiperiodic attractors appear. With further increase of *c*, asynchronous chaotic attractors, developed from the asynchronous quasiperiodic attractors, born at the upper and lower branches of H_1, disappear through boundary crises at the upper (solid triangle) and lower (open triangle) crisis curves, respectively. As an example, consider the case of $\alpha=0.75$. When crossing the curve *B* for $c\simeq1.352$, an abrupt collapse of the synchronous state occurs through a subcritical blow-out bifurcation, and then typical trajectories, starting near the synchronization line, are divergent to infinity. However, as the upper branch of D_1 is passed for $c=1.647,\ldots,$ a stabilized asynchronous period-1 attractor appears with its basin. With further increase of *c*, this asynchronous period-1 attractor is transformed into an asynchronous quasiperiodic attractor when the upper branch of H_1 is crossed at $c=1.784,\ldots.$ Finally, the asynchronous chaotic attractor, developed from the asynchronous quasiperiodic attractor, disappears suddenly with its basin through a boundary crisis, occurring for $c\simeq1.869$ at the curve (denoted by the solid triangles).

IV. SUMMARY

We have investigated how the asymmetry of coupling affects the bifurcation mechanism for the loss of synchronous chaos with varying the asymmetry parameter in two coupled 1D maps. It has been thus found that the asymmetry leads to the change in the bifurcation scenarios of the synchronization loss only for the case of symmetry-breaking pitchfork bifurcations. For the weak-coupling case, pitchfork bifurcations of asynchronous periodic saddles are replaced with saddle-node bifurcations, while for the strong-coupling case, pitchfork bifurcations of synchronous periodic saddles transform to the transcritical bifurcations. As the asymmetry parameter α is increased from 0 to 1, the effects of the saddle-node and transcritical bifurcations vary depending on their types. For example, the effect of the transcritical bifurcation depends on whether or not it induces a contact between the SCA and its basin boundary. Generally, the bifurcation effects for small α are similar to those in the symmetric-coupling case ($\alpha=0$) [7], although the underlying bifurcation mechanisms are different. However, as α is further increased, they change qualitatively, and eventually become similar to those in the unidirectionally coupled case ($\alpha=1$) [10]. Finally, we conjecture that the above results obtained in asymmetrically coupled 1D maps may be applied to a large class of real asymmetrically coupled systems, consisting of period-doubling subsystems, because the 1D map is a typical period-doubling system, exhibiting universal behavior. However, to explicitly examine our conjecture is beyond the scope of the present paper, and hence, such a work will be investigated in future.

ACKNOWLEDGMENT

This work was supported by the Korea Research Foundation under Grant No. 2000-041-D00067.

[1] H. Fujisaka and T. Yamada, Prog. Theor. Phys. **69**, 32 (1983).
[2] A.S. Pikovsky, Z. Phys. B: Condens. Matter **50**, 149 (1984).
[3] L.M. Pecora and T.L. Carroll, Phys. Rev. Lett. **64**, 821 (1990).
[4] K.M. Cuomo and A.V. Oppenheim, Phys. Rev. Lett. **71**, 65 (1993); L. Kocarev, K.S. Halle, K. Eckert, L.O. Chua, and U. Parlitz, Int. J. Bifurcation Chaos Appl. Sci. Eng. **2**, 973 (1992); L. Kocarev and U. Parlitz, Phys. Rev. Lett. **74**, 5028 (1995); N.F. Rulkov, Chaos **6**, 262 (1996).
[5] P. Ashwin, J. Buescu, and I. Stewart, Nonlinearity **9**, 703 (1996).
[6] Y.-C. Lai, C. Grebogi, J.A. Yorke, and S.C. Venkataramani, Phys. Rev. Lett. **77**, 55 (1996).
[7] V. Astakhov, A. Shabunin, T. Kapitaniak, and V. Anishchenko, Phys. Rev. Lett. **79**, 1014 (1997).
[8] Yu.L. Maistrenko, V.L. Maistrenko, A. Popovich, and E. Mosekilde, Phys. Rev. E **57**, 2713 (1998); **60**, 2817 (1999).
[9] Yu.L. Maistrenko, V.L. Maistrenko, A. Popovich, and E. Mosekilde, Phys. Rev. Lett. **80**, 1638 (1998); G.-I. Bischi and L. Gardini, Phys. Rev. E **58**, 5710 (1998).
[10] S.-Y. Kim and W. Lim, Phys. Rev. E **63**, 026217 (2001).
[11] P. Ashwin, J. Buescu, and I. Stewart, Phys. Lett. A **193**, 126 (1994); J.F. Heagy, T.L. Carroll, and L.M. Pecora, Phys. Rev. E **52**, 1253 (1995); S.C. Venkataramani, B.R. Hunt, E. Ott, D.J. Gauthier, and J.C. Bienfang, Phys. Rev. Lett. **77**, 5361 (1996); S.C. Venkataramani, B.R. Hunt, and E. Ott, Phys. Rev. E **54**, 1346 (1996).
[12] J.C. Alexander, J.A. Yorke, Z. You, and I. Kan, Int. J. Bifurcation Chaos Appl. Sci. Eng. **2**, 795 (1992); E. Ott, J.C. Sommerer, J.C. Alexander, I. Kan, and J.A. Yorke, Phys. Rev. Lett. **71**, 4134 (1993); J.C. Sommerer and E. Ott, Nature (London) **365**, 136 (1993); E. Ott, J.C. Alexander, I. Kan, J.C. Sommerer, and J.A. Yorke, Physica D **76**, 384 (1994); J.F. Heagy, T.L. Carroll, and L.M. Pecora, Phys. Rev. Lett. **73**, 3528 (1994).
[13] J. Milnor, Commun. Math. Phys. **99**, 177 (1985).
[14] E. Ott and J.C. Sommerer, Phys. Lett. A **188**, 39 (1994); Y. Nagai and Y.-C. Lai, Phys. Rev. E **56**, 4031 (1997).
[15] H. Fujisaka and T. Yamada, Prog. Theor. Phys. **74**, 918 (1985); N. Platt, E.A. Spiegel, and C. Tresser, Phys. Rev. Lett. **70**, 279 (1993); J.F. Heagy, N. Platt, and S.M. Hammel, Phys. Rev. E **49**, 1140 (1994).
[16] I. Aranson, D. Golomb, and H. Sompolinsky, Phys. Rev. Lett. **68**, 3495 (1992); D. Auerbach, *ibid.* **72**, 1184 (1994); Y. Jiang and P. Parmananda, Phys. Rev. E **57**, 4135 (1998).
[17] C. Mira, L. Gardini, A. Barugola, and J.-C. Cathala, *Chaotic Dynamics in Two-Dimensional Noninvertible Maps* (World Scientific, Singapore, 1996); R.H. Abraham, L. Gardini, and C. Mira, *Chaos in Discrete Dynamical Systems* (Springer, New York, 1997).
[18] J.D. Farmer, Phys. Rev. Lett. **55**, 351 (1985).
[19] J. Guckenheimer and P. Holmes, *Nonlinear Oscillations, Dynamical Systems, and Bifurcations of Vector Fields* (Springer, New York, 1983), p. 149.